SAS Solution Structures of the Apo and Mg^{2+}/BeF_3^--Bound Receiver Domain of DctD from *Sinorhizobium meliloti*†

B. Tracy Nixon,*,‡ Hemant P. Yennawar,‡ Michaeleen Doucleff,§ Jeffrey G. Pelton,§ David E. Wemmer,§ Susan Krueger,|| and Elena Kondrashkina⊥

Department of Biochemistry and Molecular Biology, The Pennsylvania State University, University Park, Pennsylvania 16802, Physical Biosciences Division, Lawrence Berkeley National Laboratory, Berkeley, California 94720, Department of Chemistry, University of California, Berkeley, California 94720, NIST Center for Neutron Research, National Institutes for Standards and Technology, 100 Bureau Drive, Stop 8562, Gaithersburg, Maryland 20899, and BioCAT at APS/Argonne National Laboratory, Illinois Institute of Technology, 9700 South Cass Avenue, Argonne, Illinois 60439

Received June 13, 2005; Revised Manuscript Received August 30, 2005

ABSTRACT: Two-component signal transduction is the predominant information processing mechanism in prokaryotes and is also present in single-cell eukaryotes and higher plants. A phosphorylation-based switch is commonly used to activate as many as 40 different types of output domains in more than 6000 two-component response regulators that can be identified in the sequence databases. Previous biochemical and crystallographic studies showed that phosphorylation of the two-component receiver domain of DctD causes a switch between alternative dimeric forms, but it was unclear from the crystal lattice of the activated protein precisely which of four possible dimeric configurations is the biologically relevant one [Park, S., et al. (2002) *FASEB J. 16,* 1964−1966]. Here we report solution structures of the apo and activated DctD receiver domain derived from small angle scattering data. The apo dimer closely resembles that seen in the crystal structure, and the solution data for the activated protein eliminate two of the possible four dimeric conformations seen in the crystal lattice and strongly implicate one as the biologically relevant structure. These results corroborate the previously proposed model for how receiver domains regulate their downstream AAA+ ATPase domains.

Two-component signal transduction is a predominant form of information processing in bacteria. It is also present in archae, fungi, and plants. Currently, 6600 two-component response regulators are identified in the Pfam database (*1*). In these proteins, transient phosphorylation of the "receiver" domain alters its interaction with one of some 40 different types of output domains to activate the output function, which typically regulates gene transcription. More than 400 two-component regulators are σ54-dependent transcriptional activators that usually bind as dimeric proteins to upstream promoter elements where they are poised to interact with nearby closed complexes of σ54-RNA polymerase (*2*). Upon phosphorylation of their receiver domains, these AAA+ ATPases[1] assemble into larger ring structures to activate their ATPase and transcription functions (*3*).

DctD is a σ54-dependent AAA+ ATPase that is important for biological nitrogen fixation in *Sinorhizobium meliloti* (*4*−*6*). Previous crystallographic (*7*, *8*) and biochemical (*9*) studies showed that the receiver domain of DctD is dimeric and that phosphorylation switches between alternate dimeric conformations. However, the biochemical studies suggested complex solution states, and the crystal lattice of the receiver domain bound to BeF_3^- [which mimics phosphorylation (*10*)] contained four possible dimeric conformations (see Figure 5A in ref *8*, or Figure 1 of the Supporting Information). One of these conformations (dimer A:E in ref *8*) is very similar to the dimeric structure of the phosphorylated FixJ receiver domain (*11*), another type of response regulator also present in *S. meliloti*. Therefore, this dimeric form was tentatively proposed to be the biologically relevant one for the activated receiver domain of DctD (*8*).

Recently, these crystal structures of the apo and activated forms of the DctD receiver domain were combined with

† This work was supported by NSF Grant MCB-9727745 to B.T.N., Seed Grant INNOV-TN to B.T.N. from the Huck Institute of the Pennsylvania State University, and Subcontract 6712513 from the DOE Lawrence Berkeley National Laboratory. Use of the Advanced Photon Source was supported by the U.S. Department of Energy, Basic Energy Sciences, Office of Science, under Contract W-31-109-ENG-38. BioCAT is a National Institutes of Health-supported Research Center (Grant RR-08630).

* To whom correspondence should be addressed: 156 N. Frear Lab, Biochemistry and Molecular Biology, The Pennsylvania State University, University Park, PA 16802. Phone: (814) 865-3679. Fax: (814) 863-7024. E-mail: btn1@psu.edu.

‡ The Pennsylvania State University.

§ Lawrence Berkeley National Lab and University of California.

|| National Institutes for Standards and Technology.

⊥ Illinois Institute of Technology.

[1] Abbreviations: AAA+ ATPase, member of the extended family of ATPases associated with cellular activities; APS, Advanced Photon Source at the Argonne National Laboratory (Argonne, IL); BioCAT, Biophysics Collaborative Access Team; Co−NTA or cobalt−NTA, cobalt-immobilized metal affinity chromatography resin; GuHCl, guanidine hydrochloride; HEPES, *N*-(2-hydroxyethyl)piperazine-*N*′-2-ethanesulfonic acid; HSQC, heteronuclear single-quantum correlation; NSD, normalized spatial discrepancy; NIST, National Institutes of Standards and Technology; NMR, nuclear magnetic resonance; Pfam, protein families database of alignments and HMMs; SANS, small-angle neutron scattering; SAXS, small-angle X-ray scattering; TCEP, tris-(2-carboxyethyl)phosphine hydrochloride; WAXS, wide-angle X-ray scattering.

10.1021/bi051129u CCC: $30.25
Published on Web 10/04/2005

crystal structures of the σ54-dependent activator NtrC1 of *Aquifex aeolicus* to propose how two-component signal transduction could regulate assembly of the DctD and NtrC1 AAA+ ATPase domains (*3*). In this model, the unphosphorylated receiver and ATPase domains form a dimer that holds the ATPase domain in an inactive conformation. Phosphorylation of the receiver domain stabilizes it in an alternate dimer state (dimer A:E), which frees the ATPase domains to rearrange and oligomerize to the active conformation. Thus, determining which active DctD dimer form is present in solution is important for corroborating this model.

Here we report SANS and SAXS/WAXS solution studies of the DctD receiver domain. These results strongly support prior assignments of the biologically relevant dimer conformations for apo and BeF_3^--bound forms of the receiver domain, thus strengthening the proposed model of how DctD-like receiver domains negatively control their downstream AAA+ ATPase domains.

EXPERIMENTAL PROCEDURES

Proteins. The DctD(1−143:His6) protein was prepared as previously described (*7*). Mutations were introduced into codons 136 and 137 to convert them to a *Hin*DIII restriction site to move the His_6 tag from immediately after residue 143 to immediately after residue 136. The resulting protein was purified in the same way as the longer form, using Co−NTA affinity and MONO-Q ion exchange chromatography. Protein labeled uniformly with ^{15}N was prepared using minimal medium as described previously (*9*), with purified protein being desalted against water by size exclusion chromatography and lyophilized to dryness. Protein was dissolved to a concentration of 550 μM by being gently swirled in buffer [5 mM HEPES (pH 7.0)]. Light precipitation was observed when TCEP (pH 7, final concentration of 1 mM) was subsequently added. One microliter of 10 M NaOH was added, completely dissolving the precipitated protein and bringing the pH to 7.6. Aliquots of a stock solution (40 mM $MgCl_2$, 40 mM $BeCl_2$, and 160 mM NaF dissolved in water) were added to introduce Mg^{2+}/BeF_3^-. Samples were centrifuged at 98 100 m/s^2 (10000*g*) for 5 min at room temperature and passed through an Anotop 0.1 micron filter (Whatman) prior to collection of NMR data on a DRX 500 MHz spectrometer at the indicated temperatures. Data were processed using NMRPipe (*12*) and analyzed using NMRView (*13*). For neutron and later X-ray scattering experiments, proteins were desalted or dialyzed exhaustively into final buffer [50 mM Tris-HCl (pH 8.0), 300 mM NaCl, and 10 mM TCEP]. Initial X-ray scattering experiments were conducted on samples in 10 mM HEPES buffer (pH 7.0). Buffers were made with water or 100% ^2H_2O. No adjustments were made for determining the "pH" for the ^2H_2O buffers, which were calculated to be 97% ^2H_2O after addition of the small amounts of water-based components. Samples with and without Mg^{2+}/BeF_3^- were kept on ice for up to 12 h prior to centrifugation at 1047 rad/s (10 000 rpm) for 5 min and passage through an Anotop 0.1 micron filter (Whatman) before being placed in neutron or X-ray beams. Protein concentrations were determined by the absorbance at 280 nm in 7.6 M GuHCl using an extinction coefficient of 1200 M^{-1} cm^{-1} that was derived from the primary sequence using SEDNTERP (*14*).

SAS Data Collection and Processing. SANS measurements were performed on the NG7 30-meter SANS instrument at the NIST Center for Neutron Research (*15*). The neutron wavelength, λ, was 6 Å, with a wavelength spread, $\Delta\lambda/\lambda$, of 0.15. The samples were measured for 6 h at room temperature in quartz cuvettes with a 0.1 cm path length for samples measured in H_2O buffers and a 0.2 cm path length for samples measured in ^2H_2O buffers. Scattered neutrons were detected with a 64 cm × 64 cm two-dimensional position sensitive detector with 128 × 128 pixels and a resolution of 0.5 cm per pixel. Raw counts were normalized to a common monitor count and corrected for empty cell counts, ambient room background counts, and nonuniform detector response. Data were placed on an absolute scale by normalizing the scattered intensity to the incident beam flux. Finally, the data were radially averaged to produce scattering intensity, $I(q)$, versus q curves, where $q = 4\pi \sin(\theta)/\lambda$ and 2θ is the scattering angle. Sample-to-detector distances of 5 and 1.5 m were used to cover the q range from 0.025 to 0.25 $Å^{-1}$. The scattered intensities from the samples were then further corrected for buffer scattering and incoherent scattering from hydrogen in the samples. Protein concentrations were 3.2 mg/mL for DctD(1−136:His6) and 4.6 mg/mL for DctD-(E121K:1−136:His6), with an uncertainty of ∼5%. Using these concentrations, a known scattering contrast $\Delta\rho$, and I_0 values estimated from Guinier plots, molecular weights were calculated using the formula $Mwt = (I_0 N_A)/[c(\Delta\rho v_{bar})^2]$ [where I_0 is in inverse centimeters estimated from the Guinier plot, N_A is Avogadro's number of particles per mole, the protein concentration c is in grams per cubic centimeter, contrast $\Delta\rho$ as 3.44×10^{10} cm^{-2} for protein in ^2H_2O, and the partial specific volume, v_{bar}, was 0.7419 cm^3/g calculated from sequence using SEDNTERP (*14*)].

SAXS data were collected on BioCAT undulator beamline 18-ID at the APS (*16*). Samples were exposed to focused X-rays (12 keV and a flux of 2×10^{12} photons/s after 10-fold attenuation) for 5.2 s, or for 0.6 s without attenutation (12 keV and a flux of 2×10^{13} photons/s). To determine radiation damage effects, five exposures of 0.6 s were taken for sample solutions that were pumped through a 1.5 mm quartz capillary (*17*) at 12.5 μL/s, followed by five exposures for the same sample held stationary. For all other measurements, the sample solutions were pumped through the capillary at 4 μL/s. Two-dimensional scattering patterns were obtained by using a 5 cm × 9 cm charge-coupled device (CCD) detector (*18*) at a specimen to detector distance of 2.78 m (SAXS) or 0.16 m (WAXS). Scattering intensity profiles over the q range from 0.004 to 0.800 $Å^{-1}$ were calculated from radial averaging of the two-dimensional scattering patterns using the routines in the FIT2D data analysis program (*19*), or using macros written by the APS staff for IGOR Pro (WaveMetrics, Inc.). Scattering profiles from protein with buffer and from buffer alone were scaled using incident flux values integrated over the exposure time. Protein scattering profiles were then obtained by subtracting the average of five buffer profiles from five profiles of buffer with protein. PRIMUS (*20*) was used to merge SAXS and WAXS scattering data and to calculate the radius of gyration (R_G) and forward scattering intensity (I_0). The latter was put on the absolute scale using scattering data for a known concentration of cytochrome *c* that were collected immediately before the scattering data for DctD proteins (the

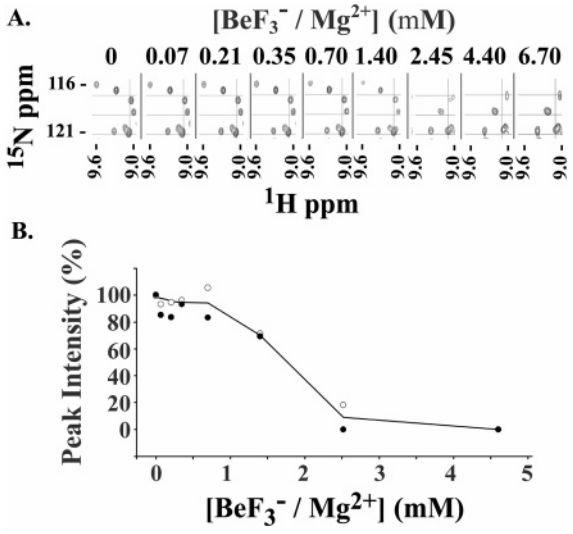

FIGURE 1: Titration of Mg^{2+}/BeF_3^-. $^1H-^{15}N$ correlation spectroscopy measurements were used to monitor ligand binding to DctD-(1−143:His6). (A) A small region illustrating how a decrease or increase in the intensities of some spectral peaks reveals conformational change upon binding of the ligand at 37 °C. (B) Intensities vs ligand concentration for the peaks at 9.6 ppm × 116 ppm and 9.3 ppm × 117 ppm (which, among others, disappeared upon binding of Mg^{2+}/BeF_3^-).

same equation described above was used to calculate molecular weight except that the value of Δp was changed to 2.67×10^{10} cm^{-2} to reflect the use of X-rays instead of neutrons). Interatomic distance distribution functions [$p(R)$] were obtained using GNOM (*21*), and they were processed to yield dummy atom structures using DAMMIN (*22*) or GASBOR (*23*). Some of the latter computations were performed on the LionXL and LionXM clusters maintained by the Penn State Center for Academic Computing. CRYSON (*24*), CRYSOL (*25*), and xtal2sas (S. Krueger and S. K. Gregurick, private communication) were used to calculate scattering curves from crystal structure models, and to fit SANS data to models. Rigid body fitting was performed using the output from these programs and MASSHA (*26*), and a global search for the optimal location of subunits in a *P*2 symmetric homodimer given the monomer structure and scattering data was performed using GLOBSYM (*27*).

RESULTS

Mg^{2+}/BeF_3^- Saturates DctD(1−143:His6) at 5 mM. Binding of Mg^{2+}/BeF_3^- can be used to mimic phosphorylation as a method for activating the DctD receiver domain (*7*−*10*). $^1H-^{15}N$ correlation spectra were used to identify chemical shifts that accompanied binding of the ligand. Useful spectra, not seen at 10 °C apparently due to aggregation, were observed at room temperature, but clusters of peaks were more sharply delineated by increasing the temperature to 37 or 42 °C (Figure 2 of the Supporting Information). Comparing spectra for protein in the absence and presence of 5 mM Mg^{2+}/BeF_3^- revealed several well-separated peaks unique to the apo or ligand-bound forms of the protein (examples are shown in Figure 1A). Quantifying exemplary peak intensities showed that the transition from the apo to ligand-bound form was essentially complete at >5 mM BeF_3^- (Figure 1B). These studies were conducted at 37 °C; less complete data for binding at 25 °C yielded similar results (not shown).

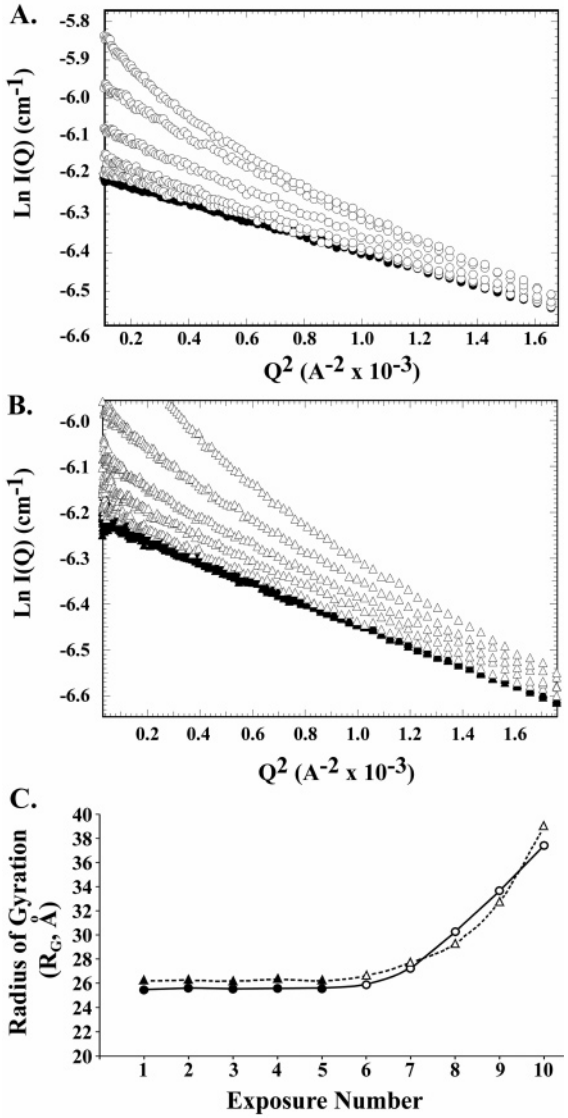

FIGURE 2: Guinier plots of flowing vs stationary solutions of DctD-(1−143:His6). Ln[$I(Q)$] vs Q^2 plots are shown for five 0.6 s exposures of a protein solution flowing at 12.5 μL/s (filled symbols) or being held stationary (empty symbols). The apo form is shown in panel A (circles), and protein activated by 5 mM Mg^{2+}/BeF_3^- is shown in panel B (triangles). Panel C shows the calculated R_G value ($Q_{max}R_G = 1.00$) for each exposure, where numbers 1−5 are for the flowing solution and 6−10 are for the stationary solution.

Flowing Sample Solutions Minimized Radiation Damage. Experiments were performed to determine conditions that minimized radiation damage to DctD(1−143:His6) protein, in both its apo and activated forms. Solutions of protein in the presence or absence of saturating amounts of Mg^{2+}/BeF_3^- were exposed to the beam for 0.6 s while being pumped through the capillary at a rate of 12.5 μL/s for five successive exposures, or then held stationary for five additional exposures. Flowing the solutions was intended to provide fresh samples for each measurement and effectively reduce exposure time by a factor of 17.4, reducing the absorbed dose from 130 to ~7 kGy (*28*). A comparison of the radius of gyration (R_G) calculated from Guinier plots (Figure 2) showed that the five exposures for moving samples were very reproducible, giving R_G values of 25.6 ± 0.1 and 26.2 ± 0.1 Å for the apo and activated protein, respectively. The first stationary exposure gave slightly larger R_G values (25.9

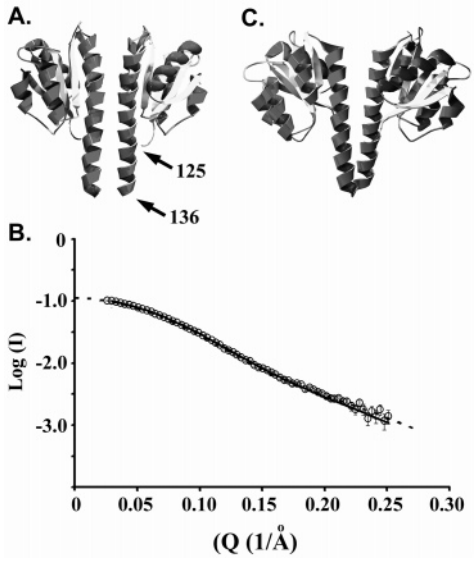

FIGURE 3: SANS data for DctD(1−136:His6). (A) Crystal structure model for deletion of residues 137−143 to shorten the helical linker. (B) A plot of log(*I*) vs *Q* (○; ±standard error) is shown together with best fit solutions for the crystal structure model determined with adjustment of the scattering length density for the hydration layer (—; CRYSON) or without the adjustment (- - -, xtal2sas). (C) Homodimer model derived by MASSHA that best fits the scattering data.

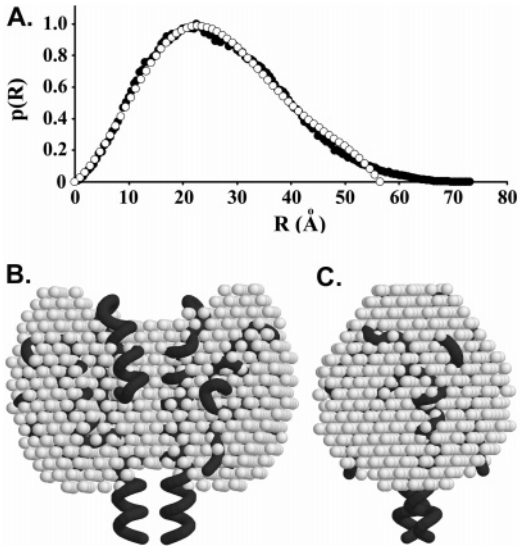

FIGURE 4: Solution dimer models for DctD(1−136:His6). (A) *p*(*R*) distribution functions from GNOM (○; ±standard error; 56 Å D_{max}) and xtal2sas (●; ±standard error) (note that the error bars fall within the data points). (B) Overlay of the crystal structure model with a low-resolution ab initio solution structure derived by DAMMIN using the 56 Å-based *p*(*R*) distribution function calculated by GNOM. (C) Same image as in panel B, rotated 90° on the vertical axis.

Å for the apoprotein and 26.6 Å for the activated protein), but successive exposures 2−5 showed dramatically increased R_G values. A slower flow rate of 4 μL/s similarly minimized the radiation damage (data not shown), and it was used in the SAXS experiments reported below.

Residues 137−143 of the Apo Form of DctD(1−143:His6) Mediate Formation of a Larger Oligomer. The R_G value of 26.2 Å seen for the activated form of the protein is similar to those that are calculated for two of the four dimer configurations seen in the crystal lattice of the Mg^{2+}/BeF_3^--bound protein (24.9, 25.3, 23.9, and 23.0 Å for A−E, A−B, A−C, and A−D dimers, respectively; note that the models lack the 13 carboxy-terminal amino acid residues which are unstructured in the crystal). However, the R_G value of 25.6 Å seen for the apo form of the protein is considerably larger than the value of 21.7 Å predicted for dimers from the crystal structure. In the crystal lattice of the off-state protein, the last six residues of the C-terminal helices of the dimeric protein bundle together to form a tetramer (*7*). Although prior ultracentrifugation studies conducted with up to 2.7 mg/mL protein showed no evidence of particles larger than dimer, these SAXS studies were conducted with 8.0 mg/mL protein. Reasoning that there might be a small amount of the tetramer seen in the crystal lattice forming in solution at this concentration of protein, we removed the last six residues by making DctD(1−136:His6). In this construction, residues 108−136 are still predicted to form a long helix, with residues 124−136 extending beyond the globular portion of the receiver domain (Figure 3A). In the truncated region, there is only one leucine that makes a small surface area contact between the two helices in the "off" state, which is lost in the "on" state; therefore, we do not expect the truncation to make any significant difference in the energetics of activation (and hence the response to BeF_3^-). Guinier analysis of SAXS data (spanning a *q* range of 0.0055−0.155 $Å^{-1}$; not shown) from the qR_G range of 0.3−1.3 estimated an R_G of 23.4 ± 0.1 Å for apo DctD(1−136:His6) and 26.3 ± 0.1 Å for the protein incubated with Mg^{2+}/BeF_3^- (5 mM). Forward scattering intensities adjusted to the absolute scale [(1.57 ± 0.08) × 10^{-2} and (1.59 ± 0.08) × 10^{-2} cm^{-1}] yielded molecular weights of 32 684 ± 1500 and 33 087 ± 1500 for the apo and activated proteins, respectively. These values are essentially identical to the molecular weight calculated for dimers from the amino acid sequence (32 280).

SANS Studies of DctD(1−136:His6). To confirm the results given above, the truncated protein was studied in SANS experiments (Figure 3B), yielding 34 600 ± 2200 for its molecular weight, which gives an aggregation number of 2.1 ± 0.2 monomers per particle. The R_G estimated by Guinier analysis (21.1 ± 0.3 Å) is also close to the value calculated with CRYSON using a model derived by truncating the crystal structure (18 Å; note that this model lacks the 13-residue His_6 tag). Using CRYSON or xtal2sas, the scattering data fit very well to the proposed biological dimer of the crystal lattice (CRYSON yielded an R_G value of 19.8 Å with a χ, variance of fit, of 1.98). Further, rigid body analysis starting with the monomer of the asymmetric unit of the crystal structure gave a very similar homodimer conformation (Figure 3C).

The truncated model predicts a maximum particle dimension (D_{max}) of 58 Å. The xtal2sas and GNOM programs differ in how they treat D_{max}: in xtal2sas it is adjusted as a parameter, while in GNOM it is fixed by the user. GNOM also calculates a "total score" based on several *p*(*R*) features that have been shown by the program author's experience to be typical of good solutions (*21*). The xtal2sas program showed a D_{max} of 74 Å, and *p*(*R*) distribution functions by GNOM (total scores of ≥0.91) were obtained using D_{max} values ranging from 55 to 74 Å, with the best occurring at 56 Å (Figure 4A).

Except for the ends of the helical tails, the truncated model for the DctD(1−136:His6) protein superimposed well onto ab initio shapes determined by simulated annealing using a single-phase dummy atoms model [DAMMIN; results for the 56 Å $p(R)$ function are shown in Figure 4B]. This suggests that the C-terminal end of the pseudo-coiled coil structure seen for the linker helices in the crystal lattice is less stable in solution.

For comparison with the crystal structure of the Mg^{2+}/BeF_3^--bound protein [which is only available for the receiver domain bearing the amino acid substitution E121K (*8*)], data were also collected for the apo form of the substitution variant DctD(E121K:1−136:His6) (data not shown). Scattering from this protein gave a molecular weight of 35 800 ± 1700 for an aggregation number of 2.2 ± 0.1 monomers per particle, an R_G of 20.3 ± 0.2 Å, and $p(R)$ distribution functions with GNOM total scores of ≥0.92 over the D_{max} range of 55−70 Å, and ab initio shapes that were also very consistent with crystal structure of the apo dimer (e.g., the root-mean-square deviation between the modeled scattering curve and the raw data processed at a D_{max} of 58 Å was 0.889).

SANS Data Suggest that Activation of DctD(1−136:His6) with Mg^{2+}/BeF_3^- Stabilizes the Predicted Alternative Dimeric Conformation. Neutron scattering was assessed for both DctD(1−136:His6) and DctD(E121K:1−136:His6) incubated with 5 mM Mg^{2+}/BeF_3^-. The I_0 values gave estimated molecular weights of 31 300 ± 1500 for DctD(1−136:His6) and 38 200 ± 1900 for DctD(E121K:1−136:His6), for aggregation numbers of 1.9 ± 0.1 and 2.4 ± 0.2 monomers per molecule, respectively. R_G values were estimated to be 22.4 ± 0.2 and 23.2 ± 0.3 Å, respectively. Each of the four dimeric models seen in the on-state crystal lattice modeled the resulting data better than the off-state dimer model (Figure 5A). Models for A−E and A−B dimers had better variances of fit (χ values of 2.08 and 1.61, respectively) than did models for A−C and A−D dimers (χ values of 4.48 and 3.18, respectively). Two of the on-state models (A−E dimer and A−B dimer) could be combined with the off-state model in weighted fitting to reduce the variance of fit (Figure 5B). The best fits were obtained with a mixture containing 20−30% of the off-state dimer. The GLOBSYM program, which globally searches for the best location of a second subunit given a monomer atomic model and point symmetry (*27*), found the best-fit homodimer with $P2$ symmetry to be very similar to the A−E dimer (χ, a measure of the discrepancy between experimental and model scattering curves, was 1.023 for the best fit vs 1.076 for the next closest fit; Figure 6). Ab initio shapes derived from GNOM and DAMMIN analyses were most consistent with high-resolution models for A−E and A−B dimers but did not distinguish between them (analyses not shown).

High-Resolution SAXS/WAXS Data Yielded Solution Structures for Off-State and On-State Dimer A−E Conformations. The neutron scattering data reported above spanned the q range from 0.025 to 0.25 $Å^{-1}$ (corresponding to a range from 250 to 25 Å in real space). This limited ab initio shape determinations for the method of simulated annealing of single-phase dummy atom models. If higher-resolution data are available, simulated annealing can be used to find a chain compatible distribution of dummy atoms. SAXS/WAXS data reaching to 0.8 $Å^{-1}$ (corresponding to 8 Å in real space) were obtained for apo and Mg^{2+}/BeF_3^--bound forms of the DctD(1−136:His6) protein (Figure 7A). Inverse Fourier transforms did not clearly reveal optimal D_{max} values, but very similar ab initio shapes were obtained independent of the D_{max} values used to generate $p(R)$ distributions over the

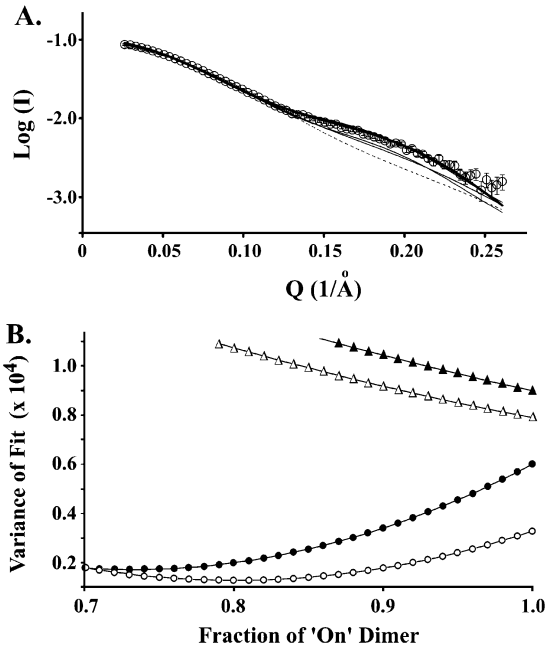

FIGURE 5: SANS data for DctD(1−136:His6) in the presence of Mg^{2+}/BeF_3^-. (A) Neutron scattering was measured for protein in the presence of the ligand (○; ±standard error) and fit using CRYSON to the crystal structure models for off-state dimer (- - -) and on-state A−E dimers (thick solid line), or A−B, A−C, or A−D dimers (thin solid lines; note that the fit to the A−B dimer closely tracks the fit to the A−E model). (B) A weighted fitting of calculated scattering curves was used to model mixtures of the off-state dimer and each of the on-state dimers. The resulting variance of fit is plotted vs the percent composition for the on-state dimer models [values go off the scale for A−C (△) and A−D (▲) models but improve for A−E (○) and A−B (●) models].

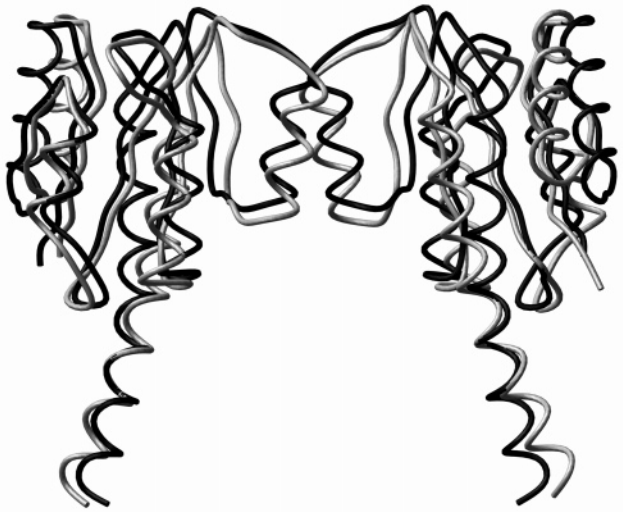

FIGURE 6: Best-fit, P_2-symmetric homodimer for DctD(1−136:His6). The SANS data in Figure 5 were used with GLOBSYM to globally search for the location of a second monomer in P_2 symmetry space that best fit the data. The resulting model (black) is shown superimposed on the crystal structure model of the A−E dimer (gray; the rmsd for the 264 Cα atoms in this alignment is 3.27 Å).

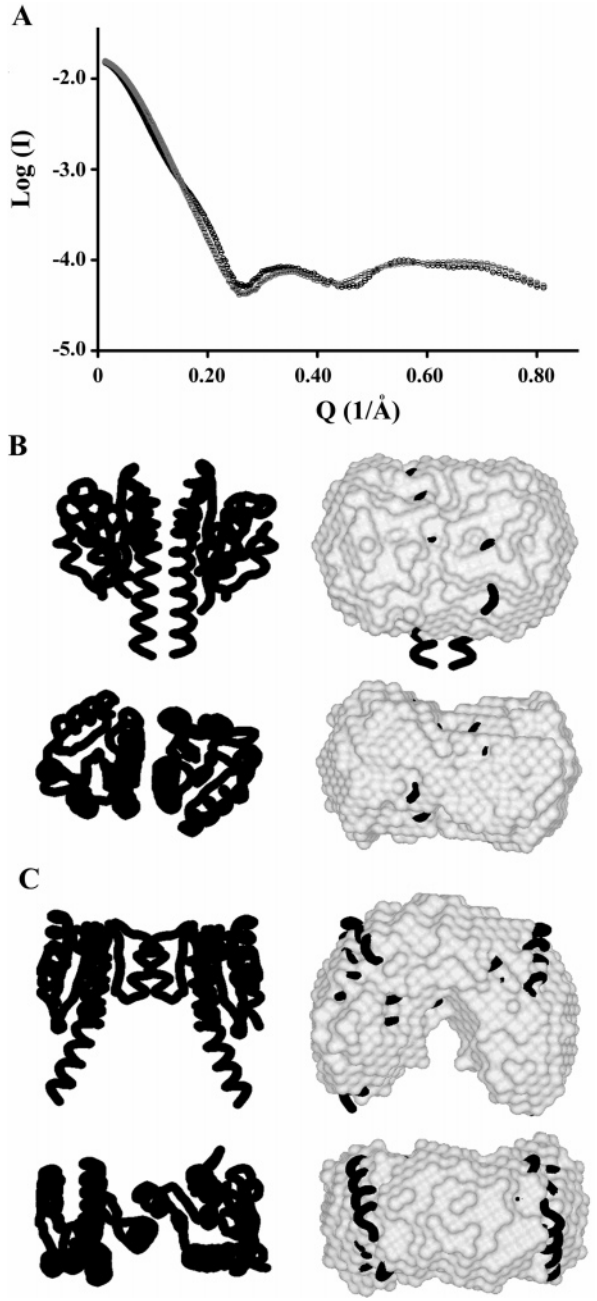

FIGURE 7: SAXS/WAXS data for DctD(1−136:His6). X-ray scattering data (A) were collected for the protein in the absence (black; ±standard error) and presence (gray; ±standard error) of 5 mM Mg^{2+}/BeF_3^- (note that error bars fall within the data points). Eight independent models derived from GASBOR were averaged and filtered (DAMAVER and DAMFILT) to generate the most likely solution structures, which were then superimposed (SUPCOMB13) with (B) the off-state, crystal structure dimer model and (C) the on-state, crystal structure A−E dimer model. In each case, the bottom views are rotated 90° relative to the top ones.

ranges of 52−66 Å for the apoprotein and 60−74 Å for the Mg^{2+}/BeF_3^--bound protein (Figure 3 of the Supporting Information). Using SUPCOMB13 (*29*), the average [DAMAVER (*30*)] of eight such models superimposed well onto the off-state dimer model and the A−E dimer model of the on-state (normalized spatial discrepancy values of 1.46 and 1.67; Figure 7B,C). Less convincing superimpositions occurred when the other dimer models were used with the data for the Mg^{2+}/BeF_3^--bound protein [normalized spatial discrepancy values of 1.80, 1.79, and 1.74, respectively, for A−B, A−C, and A−D dimers (Figure 4 of the Supporting Information); for comparison, the normalized spatial discrepancy value for superimposing the on-state solution shape and the off-state dimer crystal structure was 1.78].

DISCUSSION

Radiation damage is a possibility that must be addressed when using the intense and highly focused beams of modern synchrotrons. Flowing of sample during exposure has been reported to reduce the amount of such damage (*18*), and this was clearly seen for the DctD(1−143:His6) protein in both apo and activated forms. It is interesting that a single exposure of the stationary solution gave nearly the same R_G estimate as exposures of flowing solutions, but that repeated stationary exposures gave increasing estimates of R_G. Since the half-life of a free radical is on the order of microseconds to nanoseconds, the radiation damage may occur in two phases, during and after the 600 ms exposure. Perhaps a threshold of damage must be achieved before the R_G of DctD(1−143:His6) is affected, or alternatively, perhaps 600 ms is not long enough for the damaged protein to enlarge or form aggregates which could appear during the several-second pause between successive exposures of the stationary solutions. During this period of time, aggregates could also adhere to the capillary surface when the solution is not flowing to replenish the sample. Finally, reproducibility in successive exposures of flowing sample does not eliminate the possibility of reproducible radiation damage. This may be the cause of the 2−4 Å increase that we saw in R_G when the DctD(1−136:His6) protein was studied by SAXS rather than by SANS (23.4 and 21.1 Å for the apoprotein and 26.3 and 22.4 Å for the activated protein, respectively). Since these studies were performed at different times and places, we cannot rule out variations in the sample preparations as an alternative explanation. Despite these differences that emerge from analysis of the lowest Q data for the SAXS and SANS experiments, the structural inferences that emerge from analysis of higher Q data were consistent for both sources of radiation.

Previously published analytical ultracentrifugation data are most consistent with a dimeric model for the activated receiver domain of DctD (*7*), but the crystal lattice of Mg^{2+}/BeF_3^--bound DctD(E121K:1−143:His6) showed four possible dimeric forms (*8*). Various other biochemical measurements suggested a complex mixture of solution conformations for phosphorylated and BeF_3^--bound forms of the wild-type receiver domain when studied at room temperature (*9*). This study indicates that some of that complexity arises from higher-order oligomer formation of the off-state protein that is mediated by the last six residues of the linker segment. Such oligomerization, possibly to a tetramer form, is probably an artifact of working with only one domain of a multidomain protein. In its natural state, the receiver domain is covalently attached to the DctD ATPase and DNA binding domains, and this arrangement should preclude oligomerization via the linker segment. This notion is consistent with the idea that the receiver domain of DctD regulates its ATPase domain as does the receiver domain in the NtrC1 protein of *A. aeolicus*. The crystal structure of a fragment of the apo-NtrC1 protein bearing both the receiver and ATPase domains shows the linker sequestered from solution and in contact with the ATPase domain of a second subunit

(*3*). The SAS data presented here for the DctD receiver domain with six residues of the linker removed are totally consistent with the reported off-state dimer structure present in the crystals, and we conclude that it represents the predominant solution form as well.

These data also strongly suggest that the predominant solution conformation present under activating conditions is similar to the A−E dimer model previously described in crystallography studies. A−E and A−B dimer models are quite similar at low resolution, but these are quite different from A−C and A−D dimer models (see Figure 1 of the Supporting Information). A−E and A−B dimer models fit the SANS data and SAXS/WAXS-based solution structures significantly better than the A−C or A−D dimer model. While the A−B dimer does fit the lower-resolution SANS data as well as the A−E dimer, the latter is found to be the best homodimer conformation in a global search for quaternary structure given a monomer model and *P*2 symmetry. Further, the A−E dimer superimposes more convincingly upon the ab initio solution model derived from higher-resolution SAXS/WAXS data. The A−E dimer model is thus most consistent with the data. This conclusion has to be tempered with the low-resolution similarity between A−E and A−B dimers and difficulties that are intrinsic to the approach (*31*). These include the facts that (a) model testing does not probe all of solution space, (b) ab initio solution structures need not in principle be unique, and (c) deriving these shapes depends on a homogeneous distribution of particles. Given these potential limitations, it is reassuring that independent ab initio shape determinations, which necessarily followed different annealing pathways, gave similar solutions. Further, very similar shapes were obtained regardless of which (reasonable) D_{max} values were used to calculate the distance distribution functions.

Additional strong but indirect support for concluding that the A−E dimer represents the solution state for the activated DctD receiver domain comes from a crystal structure of the phosphorylated, Mg^{2+}-bound receiver domain of NtrC1 that has recently been determined (Doucleff et al., *32*). It forms a dimer similar to that of the A−E dimer of the Mg^{2+}/BeF_3^--bound form of the DctD receiver domain, but its crystal lattice does not have the other alternative dimers as seen in the DctD lattice. Furthermore, WAXS data for the NtrC1 receiver domain in the off- and on-states are nearly superimposable on those reported here for the DctD receiver domain [Doucleff et al., *32*; low-angle SAXS data show that in both forms of the NtrC1 fragments the linkers interact to form tetramers rather than dimers (Nixon, unpublished observation)].

The low-resolution solution structures we report here show that the apo and active dimer states of the DctD receiver domain seen in the crystal lattice are also present in solution. The higher-resolution SAXS data (to ∼8 Å) also help to clarify which of the four Mg^{2+}/BeF_3^--bound dimers seen in the crystal lattice is the biologically relevant one. This clarification is important for reinforcing the recently proposed model for how receiver domains regulate their attached AAA+ ATPase in σ54-dependent transcriptional activators such as NtrC1 and DctD (*3*). That model depends on the receiver domain switching between dramatically different dimeric forms. The off-state dimer represses oligomer assembly of the ATPase domain by forming a large dimerization interface, predominantly along linker helix 5. In the on-state dimer (A−E dimer), the linker helices are separated, allowing the attached AAA+ ATPase domains to rearrange into the active oligomeric ring and to initiate transcription activation.

ACKNOWLEDGMENT

We thank Dmitri Svergun and Maxim Petoukhov (EMBL, Hamburg, Germany) for helpful discussions about using their software programs for SAXS/WAXS data analysis. To describe fully and accurately the materials preparation and measurement protocols of this research, it is necessary to mention certain commercial sources and products that were used. These references should not be construed as being endorsements by NIST, nor should it be inferred that the products mentioned are necessarily the best available for the purpose.

SUPPORTING INFORMATION AVAILABLE

Figures illustrating (1) the four Mg^{2+}/BeF_3^- dimer models, (2) HSQC spectra for the apoprotein at different temperatures, (3) crystal structure model for the apoprotein and for the A−E dimer of the Mg^{2+}/BeF_3^--bound protein superimposed on solution structures derived from SAXS/WAXS data at various D_{max} values, and (4) crystal structure models of A−B, A−C, and A−D dimers superimposed on the solution structure derived from SAXS/WAXS scattering data for the Mg^{2+}/BeF_3^--bound DctD(1−136:His6) protein. This material is available free of charge via the Internet at http://pubs.acs.org.

REFERENCES

1. Bateman, A., Coin, L., Durbin, R., Finn, R. D., Hollich, V., Griffiths-Jones, S., Khanna, A., Marshall, M., Moxon, S., Sonnhammer, E. L., Studholme, D. J., Yeats, C., and Eddy, S. R. (2004) The Pfam protein families database, *Nucleic Acids Res. 32*, D138−D141.
2. Zhang, X., Chaney, M., Wigneshweraraj, S. R., Schumacher, J., Bordes, P., Cannon, W., and Buck, M. (2002) Mechanochemical ATPases and transcripitonal activation, *Mol. Microbiol. 45*, 895−903.
3. Lee, S. Y., DeLaTorre, A., Yan, D., Kustu, S., Nixon, B. T., and Wemmer, D. E. (2003) Regulation of the transcriptional activator NtrC1: Structural studies of the regulatory and AAA+ ATPase domains, *Genes Dev. 17*, 2552−2563.
4. Ronson, C. W., Astwood, P. M., and Downie, A. J. (1984) Molecular cloning and genetic organization of C4-dicarboxylate transport genes from *Rhizobium leguminosarum*, *J. Bacteriol. 160*, 903−909.
5. Finan, T. M., Wood, J. M., and Jordan, D. C. (1983) Symbiotic properties of C4-dicarboxylate acid transport mutants of *Rhizobium leguminosarum*, *J. Bacteriol. 154*, 1403−1413.
6. Ronson, C. W., Astwood, P. M., Nixon, B. T., and Ausubel, F. M. (1987) Deduced products of C4-dicarboxylate transport regulatory genes of *Rizobium leguminosarum* are homologous to nitrogen regulatory gene products, *Nucleic Acids Res. 15*, 7921−7934.
7. Meyer, M., Park, S., Zeringue, L., Staley, M., McKinstry, M., Kaufman, R. I., Zhang, H., Yan, D., Yennawar, N., Yennawar, H., Farber, G. K., and Nixon, B. T. (2001) A dimeric two-component receiver domain inhibits the σ54-dependent ATPase in DctD, *FASEB J. 15*, 1326−1328.
8. Park, S., Meyer, M., Jones, A. D., Yennawar, H., Yennawar, N., and Nixon, B. T. (2002) Two-component signaling in the AAA+ ATPase DctD: Binding Mg^{2+} and BeF_3^- selects between alternative dimeric states of the receiver domain, *FASEB J. 16*, 1964−1966.

9. Park, S., Zhang, H., Jones, A. D., and Nixon, B. T. (2002) Biochemical evidence for multiple dimeric states of the *Sinorhizobium meliloti* DctD receiver domain, *Biochemistry 41*, 10934−10941.
10. Yan, D., Cho, H. S., Hastings, C. A., Igo, M. M., Lee, S. Y., Pelton, J. G., Stewart, V., Wemmer, D. E., and Kustu, S. (1999) Beryllofluoride mimics phosphorylation of NtrC and other bacterial response regulators, *Proc. Natl. Acad. Sci. U.S.A. 96*, 14789−14794.
11. Birck, C., Mourey, L., Gouet, P., Fabry, B., Schumacher, J., Rousseau, P., Kahn, D., and Samama, J. P. (1999) Conformational changes induced by phosphorylation of the FixJ receiver domain, *Struct. Folding Des. 7*, 1505−1515.
12. Delaglio, F., Grzesiek, S., Vuister, G. W., Zhu, G., Pfeifer, J., and Bax, A. (1995) NMRPipe: A multidimensional spectral processing system based on UNIX pipes, *J. Biomol. NMR 6*, 277−293.
13. Johnson, B. A. (2004) Using NMRView to visualize and analyze the NMR spectra of macromolecules, *Methods Mol. Biol. 278*, 313−352.
14. Laue, T. (2001) Biophysical studies by ultracentrifugation, *Curr. Opin. Struct. Biol. 11*, 579−583.
15. Glinka, C. J., Barker, J. B., Hammouda, B., Krueger, S., Moyer, J. J., and Orts, W. J. (1998) The 30m Small-Angle Neutron Scattering Instruments at the National Institute of Standards and Technology, *J. Appl. Crystallogr. 31*, 430−445.
16. Fischetti, R., Stepanov, S., Rosenbaum, G., Barrea, R., Black, E., Gore, D., Heurich, R., Kondrashkina, E., Kropf, A. J., Wang, S., Zhang, K., Irving, T. C., and Bunker, G. B. (2004) The BioCAT undulator beamline 18ID: A facility for biological non-crystalline diffraction and X-ray absorption spectroscopy at the Advanced Photon Source, *J. Synchrotron Radiat. 11*, 399−405.
17. Fischetti, R. F., Rodi, D. J., Mirza, A., Irving, T. C., Kondrashkina, E., and Makowski, L. (2003) High-resolution wide-angle X-ray scattering of protein solutions: Effect of beam dose on protein integrity, *J. Synchrotron Radiat. 10*, 398−404.
18. Phillips, W. C., Stewart, A., Stanton, M., Naday, I., and Ingersoll, C. (2002) High-sensitivitiy CCD-based X-ray detector, *J. Synchrotron Radiat. 9*, 36−43.
19. Hammersley, A. P. (1998) Fit2D version 9.129 Reference Manual version 3.1, ESRF Internal Report, ESRF98HA01T, ESRF, Grenoble, France.
20. Konarev, P. V., Volkov, V. V., Sokolova, A. V., Koch, M. H. J., and Svergun, D. I. (2003) PRIMUS: A Windows PC-based system for small-angle scattering data analysis, *J. Appl. Crystallogr. 36*, 1277−1282.
21. Svergun, D. I. (1992) Determination of the regularization parameter in indirect-transform methods using perceptual criteria, *J. Appl. Crystallogr. 25*, 495−503.
22. Svergun, D. I. (1999) Restoring low resolution structure of biological macromolecules from solution scattering using simulated annealing, *Biophys. J. 76*, 2879−2886.
23. Svergun, D. I., Petoukhov, M. V., and Koch, M. H. J. (2001) Determination of domain structure of proteins from X-ray solution scattering, *Biophys. J. 80*, 2946−2953.
24. Svergun, D. I., Richard, S., Koch, M. H. J., Sayers, Z., Kuprin, S., and Zaccai, G. (1998) Protein hydration in solution: Experimental observation by X-ray and neutron scattering, *Proc. Natl. Acad. Sci. U.S.A. 95*, 2267−2272.
25. Svergun, D. I., Barberato, C., and Koch, M. H. J. (1995) CRYSOL: A program to evaluate X-ray solution scattering of biological macromolecules from atomic coordinates, *J. Appl. Crystallogr. 28*, 768−773.
26. Konarev, P. V., Petoukhov, M. V., and Svergun, D. I. (2001) MASSHA: A graphics system for rigid-body modelling of macromolecular complexes against solution scattering data, *J. Appl. Crystallogr. 34*, 527−532.
27. Petoukhov, M. V., and Svergun, D. I. (2002) Rigid body modelling of symmetric oligomers, http://www.embl-hamburg.de/ExternalInfo/Research/Sax/globsymm.html.
28. Kuwamoto, S., Akiyama, S., and Fujisawa, T. (2004) Radiation damage to a protein solution, detection by synchrotron X-ray small-angle scattering: Dose-related considerations and suppression by cryoprotectants, *J. Synchrotron Radiat. 11*, 462−468.
29. Kozin, M. B., and Svergun, D. I. (2000) Automated matching of high- and low-resolution structural models, *J. Appl. Crystallogr. 34*, 33−41.
30. Volkov, V. V., and Svergun, D. I. (2003) Uniqueness of ab initio shape determination in small-angle scattering, *J. Appl. Crystallogr. 36*, 860−864.
31. Vachette, P., Koch, M. H., and Svergun, D. I. (2003) Looking behind the beamstop: X-ray solution scattering studies of structure and conformational changes of biological macromolecules, *Methods Enzymol. 374*, 584−615.
32. Doucleff, M., Chen, B., Maris, A. E., Wemmer, D. E., Kondrashkina, E., and Nixon, B. T. (2005) Negative Regulation of AAA+ ATPase Assembly by Two Component Receiver Domains: A Transcription Activation Mechanism that is Conserved in Mesophilic and Extremely Hyperthermophilic Bacteria. *J. Mol. Biol.* Published online September 14.

BI051129U